The Mechanical Properties and Elastic Anisotropy of η'-Cu6Sn5 and Cu3Sn Intermetallic Compounds

Ding, Chao; Wang, Jian; Liu, Tianhan; Qin, Hongbo; Yang, Daoguo; Zhang, Kouchi

DOI
10.3390/cryst11121562

Publication date
2021

Document Version
Final published version

Published in
Crystals

crystals

MDPI

Article

The Mechanical Properties and Elastic Anisotropy of η′-Cu_6Sn_5 and Cu_3Sn Intermetallic Compounds

Chao Ding [1,2], Jian Wang [1,2], Tianhan Liu [3], Hongbo Qin [1,2,*], Daoguo Yang [1,2] and Guoqi Zhang [2,4]

[1] Engineering Research Center of Electronic Information Materials and Devices, Ministry of Education, Guilin University of Electronic Technology, Guilin 541004, China; 19012302007@mails.guet.edu.cn (C.D.); 20012201037@mails.guet.edu.cn (J.W.); d.g.yang@guet.edu.cn (D.Y.)
[2] Guangxi Key Laboratory of Manufacturing System and Advanced Manufacturing Technology, School of Mechanical and Electronic Engineering, Guilin University of Electronic Technology, Guilin 541004, China; g.q.zhang@tudelft.nl
[3] Reliability Research and Analysis Center, No. 5 Electronics Research Institute of the Ministry of Industry and Information Technology, Advanced IC Reliability Engineering Research Center of Guangdong Province, Guangzhou 511370, China; 1801302029@mails.guet.edu.cn
[4] EEMCS Faculty, Delft University of Technology, 2628 Delft, The Netherlands
* Correspondence: qinhb@guet.edu.cn; Tel.: +86-773-2290108

Abstract: Full intermetallic compound (IMC) solder joints present fascinating advantages in high-temperature applications. In this study, the mechanical properties and elastic anisotropy of η′-Cu_6Sn_5 and Cu_3Sn intermetallic compounds were investigated using first-principles calculations. The values of single-crystal elastic constants, the elastic (E), shear (G), and bulk (B) moduli, and Poisson's ratio (ν) were identified. In addition, the two values of G/B and ν indicated that the two IMCs were ductile materials. The elastic anisotropy of η′-Cu_6Sn_5 was found to be higher than Cu_3Sn by calculating the universal anisotropic index. Furthermore, an interesting discovery was that the above two types of monocrystalline IMC exhibited mechanical anisotropic behavior. Specifically, the anisotropic degree of E and B complied with the following relationship: η′-Cu_6Sn_5 > Cu_3Sn; however, the relationship was Cu_3Sn > η′-Cu_6Sn_5 for the G. It is noted that the anisotropic degree of E and G was similar for the two IMCs. In addition, the anisotropy of the B was higher than the G and E, respectively, for η′-Cu_6Sn_5; however, in the case of Cu_3Sn, the anisotropic degree of B, G, and E was similar.

Keywords: mechanical properties; elastic anisotropic; intermetallic compounds; first-principles calculates

Citation: Ding, C.; Wang, J.; Liu, T.H.; Qin, H.; Yang, D.; Zhang, G. The Mechanical Properties and Elastic Anisotropy of η′-Cu_6Sn_5 and Cu_3Sn Intermetallic Compounds. *Crystals* **2021**, *11*, 1562. https://doi.org/10.3390/cryst11121562

Academic Editors: Pavel Lukáč, David Holec and Wojciech Polkowski

Received: 30 October 2021
Accepted: 13 December 2021
Published: 14 December 2021

1. Introduction

The application of high-powered electronic equipment and third-generation semiconductor power devices is currently widespread and requires high service temperatures (>250 °C) for solder joints [1,2]. The two common tin-based intermetallic compounds (IMCs) are Cu_6Sn_5 and Cu_3Sn, the melting point of which is 415 and 676 °C, respectively [3], and both have excellent thermodynamic and kinetic stability [1,4,5]. As such, full IMC solder joints have fascinating advantages in high-temperature application fields. Concurrently, the volume and mass of these solder joints are reduced due to high-density packaging, which enables increasing the proportion of IMCs in solder joints and creating a full IMC solder matrix. Several studies have shown that the tensile and shear strength of solder joints will be influenced by the thickness of the IMC layer [6–8]. Furthermore, hundred-micron solder joints only include a small number of grains; this will cause the solder joints to exhibit obvious anisotropic mechanical properties [9]. It follows that the mechanical properties of materials, based on large-scale specimens, will not accurately characterize the mechanical behavior of microscale solder joints. Domestic and foreign research

both present studies on the mechanical properties of Cu_6Sn_5 and Cu_3Sn. The Young's modulus (E) and hardness (H) of Cu_3Sn and Cu_6Sn_5 were measured by nanoindentation experiments [10–13]. Ghosh et al. [14] identified the values of E, shear modulus (G), bulk modulus (B), and Poisson's ratio (v) using the pulse-echo method. However, due to the influence of experimental methods, sample manufacturing processes, and mechanical anisotropy, different experimental results were reported. For example, An et al. [15] studied E anisotropy of Cu_3Sn using the first-principles method, and the results showed that the experimental results of mechanical properties will be influenced by mechanical anisotropy. Mu et al. [16] found that Cu_6Sn_5 and $(Cu, Ni)_6Sn_5$ reflected high anisotropy in E and for H. Moreover, because bulk single-crystal IMCs are difficult to prepare using the current experimental devices and methods, few reports exist on directly obtaining anisotropic mechanical properties through experiments. Choudhury et al. [17] investigated anisotropic mechanical properties for single-grain Cu_6Sn_5 using nanoindentation and electron back-scattered diffraction. However, information about anisotropic mechanical properties that were obtained through experimental methods is limited because it is difficult to obtain this information from all directions.

It is noted that first-principles methods have in recent years been applied for investigating the mechanical properties of materials, including predicting the properties of metallic systems subjected to doping [18–22]; this has, to an extent, compensated for the shortcomings of experimental methods. In addition, Cu_6Sn_5 can exist in a variety of crystal structures, i.e., η, η′, η^6, η^8, η^{4+1}, and η′′, and the η^8 and η^{4+1} superstructures are approximant structures of the incommensurate η′′ phase [23]. Importantly, η′-Cu_6Sn_5 and Cu_3Sn are the most common phase during the service of solder joints [24]; therefore, they have a significant effect on the mechanical behavior of microscale solder joints. Although the anisotropic mechanical properties of Cu_3Sn were investigated by first-principles method, the anisotropy of B and G have typically been neglected. Furthermore, simulations for detecting the anisotropic mechanical properties of η′-Cu_6Sn_5 are rare. Actually, E, B, and G represent the resistance to uniaxial stretching, volume deformation, and plastic deformation capacity, respectively. Elastic anisotropy is related to the generation of microcracks. As such, there is a need for systematically analyzing the mechanical properties and elastic anisotropy of η′-Cu_6Sn_5 and Cu_3Sn, further contributing to improving the durability of solder joints.

In this paper, the elastic constants of monocrystalline η′-Cu_6Sn_5 and Cu_3Sn were calculated based on the first-principles method. Then, according to the Voigt–Reuss–Hill approximation, the E, B, G, and v of polycrystalline could be obtained. Finally, the directional dependence and anisotropic degree of E, B, and G were investigated.

2. Computational Methods and Details

In this study, a first-principles approach, based on density functional theory integrated with the CASTEP code [25] in the Materials Studio software [26], was employed to calculate the elastic constants of single crystals. The Cu_3Sn is a large one-dimensional long-period superstructure based on a *hcp* unit cell. In order to improve computational efficiency, the crystal model established by Burkhardt et al. [27] was employed in first-principles calculations. The η′-Cu_6Sn_5 and Cu_3Sn are monoclinic and orthorhombic systems, respectively [27,28]. The atomic site parameters and lattice constants of these two IMCs is presented in existing research [27,28]. The crystal models of η′-Cu_6Sn_5 and Cu_3Sn were created as shown in Figure 1a, b, respectively.

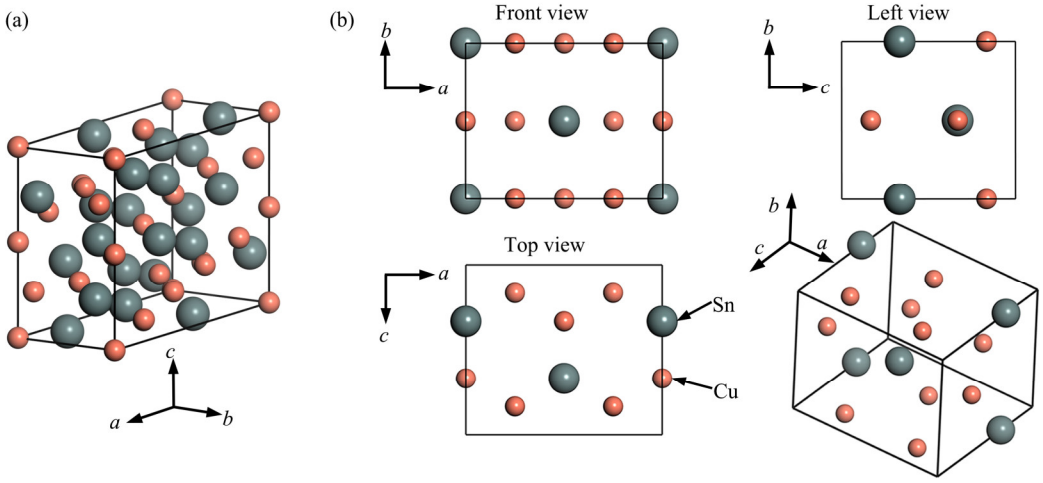

Figure 1. Crystal structures: (**a**) unit cell of monoclinic η′-Cu_6Sn_5; (**b**) three views of unit cell of orthorhombic Cu_3Sn.

The exchange-correlation energy was described by the generalized gradient approximation (GGA) with the Perdew and Wang (PW91) [29] functional for η′-Cu_6Sn_5 and Cu_3Sn. The ultrasoft pseudopotentials [30] was used to describe ionic cores for the two IMC. The Monkhorst–Pack k-points meshes were 8 × 8 × 10 and 8 × 10 × 9 for η′-Cu_6Sn_5 and Cu_3Sn, respectively. The two IMCs employed all plane-wave cutoff energy of 550 eV. The self-consistent field tolerance was set as 5.0×10^{-7} eV/atom. Once the geometric optimizations were completed, the lattice constants and the atom coordinates of the unit cells were completely relaxed, and the forces on atoms were less than 0.01 eV/Å.

3. Results and Discussion

3.1. Structural Properties

Following geometric optimization, the structural information of η′-Cu_6Sn_5 and Cu_3Sn was summarized (see Table 1). The calculated results, obtained using the GGA, showed good agreement with the experimental value. For η′-Cu_6Sn_5 and Cu_3Sn, the lattice constant errors were lower than 2.2% and 1.8%, respectively; the volume errors of unit cells were 4.4% and 1.6%, respectively. Based on the error analysis, the results of geometry optimization were reasonable.

Table 1. The lattice constants of η′-Cu_6Sn_5 and Cu_3Sn.

Structure	Method	Lattice Constants			
		a_0 (Å)	b_0 (Å)	c_0 (Å)	V_0 (Å^3)
η′-Cu_6Sn_5	GGA	11.160	7.445	9.901	813.466
	Expt. [31]	11.022	7.282	9.827	779.368
	GGA [32]	11.370	7.510	10.020	846.019
Cu_3Sn	GGA	5.391	4.278	4.795	110.586
	Expt. [15]	5.490	4.320	4.740	112.418
	GGA [33]	5.537	4.344	4.781	114.996

3.2. Elastic Properties

3.2.1. The Elastic Constants of Single Crystals

Due to the presence of anisotropy, elastic constants $\boldsymbol{C}_{ij}$ (the elastic stiffness matrix) and the elastic compliance matrix S_{ij} were important for describing the relationships between stress and strain in a single crystal. Based on the crystal symmetry, η′-Cu_6Sn_5 and Cu_3Sn had 13 and 9 independent elastic constants, respectively. The ($\boldsymbol{C}_{ij}$) is an inverse matrix of, ($\boldsymbol{S}_{ij}$), i.e., ($\boldsymbol{C}_{ij}$) = ($\boldsymbol{S}_{ij}$)$^{-1}$. In this paper, elastic constants C_{ij} and S_{ij} of η′-Cu_6Sn_5 and Cu_3Sn were calculated as shown in Tables 2 and 3. The calculated C_{ij} was in good agreement with previously calculated values and demonstrated the reasonability of the results in the present work. To ensure stable η′-Cu_6Sn_5 and Cu_3Sn crystal structures, C_{ij} should comply with the corresponding mechanical stability criteria given by Equations (1) and (2) [34], respectively. By substituting the data of Table 2 into Equations (1) and (2), the above two crystal structures were shown to be mechanically stable.

$$\begin{gathered} C_{11}>0,\ C_{22}>0,\ C_{33}>0,\ C_{44}>0,\ C_{55}>0, C_{66}>0,\ [C_{11}+C_{22}+C_{33}+2(C_{12}+C_{13}+C_{23})]>0, \\ (C_{33}C_{55}-C_{35}^2)>0,\ (C_{44}C_{66}-C_{46}^2)>0,\ (C_{22}+C_{33}-2C_{23})>0, \\ [C_{22}(C_{33}C_{55}-C_{35}^2)+2C_{23}C_{25}C_{35}-C_{23}^2C_{55}-C_{25}^2C_{33}]>0, \\ \{2[C_{15}C_{25}(C_{33}C_{12}-C_{13}C_{23})+C_{15}C_{35}(C_{22}C_{13}-C_{12}C_{23})+C_{25}C_{35}(C_{11}C_{23}-C_{12}C_{13})] \\ -[C_{15}^2(C_{22}C_{33}-C_{23}^2)+\ C_{25}^2(C_{11}C_{33}-C_{13}^2)+C_{35}^2(C_{11}C_{22}-C_{12}^2)]+C_{55}g\}>0 \\ g=C_{11}C_{22}C_{33}-C_{11}C_{23}^2-C_{22}C_{13}^2-C_{33}C_{12}^2+2C_{12}C_{13}C_{23}. \end{gathered} \tag{1}$$

$$\begin{gathered} C_{11}>0,\ C_{44}>0,\ C_{55}>0,\ C_{66}>0,\ C_{11}C_{22}>C_{12}^2, \\ C_{11}C_{22}C_{33}+2C_{12}C_{13}C_{23}-C_{11}C_{23}^2-C_{22}C_{13}^2-C_{33}C_{12}^2>0. \end{gathered} \tag{2}$$

Table 2. The C_{ij} of η′-Cu_6Sn_5 and Cu_3Sn (GPa).

Structure	C_{11}	C_{22}	C_{33}	C_{44}	C_{55}	C_{66}	C_{12}	C_{13}	C_{15}	C_{23}	C_{25}	C_{35}	C_{46}	Note
η′-Cu_6Sn_5	136.2	164.5	146.3	38.2	44.1	44.2	65.8	58.3	−10.6	63.0	0.4	−3.0	1.1	Present
	156.4	165.2	155.8	42.3	51.9	48.0	62.2	69.4	-	60.6	-	-	-	Theo. [32]
Cu_3Sn	213.6	218.6	185.0	54.2	52.3	63.1	96.8	99.4	-	108.1	-	-	-	Present
	154.6	173.7	148.2	50.2	44.2	55.0	78.9	76.5	-	95.1	-	-	-	Theo. [35]
	207.0	226.0	194.0	58.0	47.0	57.0	93.0	94.0	-	94.0	-	-	-	Theo. [15]

Table 3. The S_{ij} of η′-Cu_6Sn_5 and Cu_3Sn (×10^{-3}, GPa^{-1}).

Structure	S_{11}	S_{22}	S_{33}	S_{44}	S_{55}	S_{66}	S_{12}	S_{13}	S_{15}	S_{23}	S_{25}	S_{35}	S_{46}
η′-Cu_6Sn_5	10.13	8.19	8.92	26.20	23.20	22.63	−3.03	−2.69	2.27	−2.34	−0.95	−0.02	−0.66
Cu_3Sn	6.64	6.85	8.62	18.45	19.13	15.85	−1.65	−2.60	-	−3.11	-	-	-

3.2.2. Elastic Constants for Polycrystalline Aggregates

Mechanical properties of polycrystalline aggregate, such as *B* and *G* could be obtained by Voigt–Reuss–Hill approximation [36, 37]. The Voigt, Reuss, and Hill approximations obtain the maximum, minimum, and average value of *B* and *G*, respectively. Voigt bulk modulus B_V, Voigt shear modulus G_V, Reuss bulk modulus B_R, and Reuss shear modulus G_R can be calculated by Equations (3)–(6) [38].

$$B_V = \frac{1}{9}(C_{11} + C_{22} + C_{33}) + \frac{2}{9}(C_{12} + C_{13} + C_{23}) \quad (3)$$

$$G_V = \frac{1}{15}(C_{11} + C_{22} + C_{33} - C_{12} - C_{13} - C_{23}) + \frac{1}{5}(C_{44} + C_{55} + C_{66}) \quad (4)$$

$$B_R = [(S_{11} + S_{22} + S_{33}) + 2(S_{12} + S_{13} + S_{23})]^{-1} \quad (5)$$

$$G_R = 15[4(S_{11} + S_{22} + S_{33}) - 4(S_{12} + S_{13} + S_{23}) + 3(S_{44} + S_{55} + S_{66})]^{-1} \quad (6)$$

According to empirical formulas proposed by Hill [39], the *B* and *G* of polycrystalline aggregates satisfy Equations (7) and (8), respectively.

$$B = (B_V + B_R)/2 \quad (7)$$

$$G = (G_V + G_R)/2. \quad (8)$$

The *E* and ν of polycrystalline aggregates are defined as:

$$E = 9BG/(3B + G) \quad (9)$$

$$\nu = (3B - 2G)/(6B + 2G). \quad (10)$$

The theoretical results of *E*, *G*, *B*, and ν for η′-Cu_6Sn_5 and Cu_3Sn are summarized in Table 4. The theoretical values and the reported experimental results showed excellent consistency for Cu_3Sn. Although reports on experimental results are rare for η′-Cu_6Sn_5, the present work is supported by previously computed values (see Table 4). Therefore, in this paper, the results calculated using the first-principles method is reasonable.

Table 4. The *E* (GPa), *G* (GPa), *B* (GPa), ν, and *G*/*B* of η′-Cu_6Sn_5 and Cu_3Sn.

Structure	*E*	G_V	G_R	*G*	B_V	B_R	*B*	ν	*G*/*B*	Note
η′-Cu_6Sn_5	109.8	42.6	42.0	42.3	91.2	90.0	90.6	0.30	0.47	Present
	94.4	-	-	35.9	-	-	84.4	0.31	0.43	Expt. [14]
	116.7	-	-	45.0	-	-	95.5	-	0.47	Theo. [32]
	107.9	-	-	42.4	-	-	79.4	0.27	0.53	Theo. [20]
Cu_3Sn	143.9	54.8	53.9	54.4	136.2	135.6	135.9	0.32	0.40	Present
	123.2	-	-	46.7	-	-	113.8	0.32	0.41	Expt. [14]
	143.0	-	-	-	-	-	-	-	-	Expt. [10,40]
	147.0	-	-	56.0	-	-	132.0	0.32	0.42	Theo. [15,41]

Generally, *G*/*B* and ν [19] are employed to evaluate the brittleness of materials. If *G*/*B* > 0.57 and ν < 0.26, the materials will be brittle, or, alternatively, will show ductility. Table 4 shows that η′-Cu_6Sn_5 and Cu_3Sn all conformed to the following criterion: *G*/*B* < 0.57, ν > 0.26; as such, they were ductile materials.

3.3. Elastic Anisotropy

Elastic anisotropy is related to the generation of microcracks; it also causes poor consistency in the results of tests reviewing the mechanical properties of materials. Therefore, the investigation of elastic anisotropy related to η′-Cu_6Sn_5 and Cu_3Sn is favorable for better understanding the failure behaviors in these materials and, accordingly, improving their mechanical durability. In this paper, three anisotropic indexes were applied to assess the elastic anisotropy of η′-Cu_6Sn_5 and Cu_3Sn, i.e., universal anisotropic index A^U, as well as the anisotropic percentage in the compression (A_{comp}) and shear (A_{shear}) modes [36]. The three anisotropic indexes can be expressed as follows:

$$A^U = 5G_V/G_R + B_V/B_R - 6 \quad (11)$$

$$A_{comp} = (B_V - B_R)/(B_V + B_R) \quad (12)$$

$$A_{shear} = (G_V - G_R)/(G_V + G_R) \quad (13)$$

Furthermore, shear anisotropy in different crystal planes can be evaluated by shear anisotropy factors, i.e., A_1, A_2, and A_3 denote the anisotropic degree in the (100), (010), and (001) crystal planes, respectively [33]. The three shear anisotropy factors for the monoclinic, and orthorhombic structures can be defined as follows [33,42]:

$$A_1 = 4C_{44}/(C_{11} + C_{33} - 2C_{13}) \quad (14)$$

$$A_2 = 4C_{55}/(C_{22} + C_{33} - 2C_{23}) \quad (15)$$

$$A_3 = 4C_{66}/(C_{11} + C_{22} - 2C_{12}) \quad (16)$$

Generally, $A^U = A_{comp} = A_{shear} = 0$, and $A_1 = A_2 = A_3 = 1$, which represent isotropy; otherwise, $A^U \neq 0$, $A_{comp} \neq 0$, $A_{shear} \neq 0$, $A_1 \neq 1$, $A_2 \neq 1$, and $A_3 \neq 1$, which represent anisotropy. For A^U, A_{comp}, and A_{shear}, the deviation between 0 and actual values was used to describe the anisotropic degree. For A_1, A_2, and A_3, the deviation of from 1 represent the anisotropic degree. The calculated A^U, A_{comp}, A_{shear}, A_1, A_2, and A_3 of η′-Cu_6Sn_5 and Cu_3Sn are summarized in Table 5. The values of A^U were 0.0848 and 0.0838 for η′-Cu_6Sn_5 and Cu_3Sn, respectively, which showed that the elastic anisotropy of η′-Cu_6Sn_5 was higher. Meanwhile, the A_{comp} of Cu_3Sn were all close to 0; this indicated modest compression anisotropy. It is worth noting that the A_{shear} of η′-Cu_6Sn_5 and Cu_3Sn were 0.0071 and 0.0079, respectively, and the shear anisotropy of η′-Cu_6Sn_5 was lower. Moreover, according to the calculated values of A_1, A_2, and A_3, the shear anisotropy of η′-Cu_6Sn_5 was low and similar in three crystal planes and was the highest and lowest in the (010) and (001) planes for Cu_3Sn, respectively.

Table 5. The anisotropic indexes of η′-Cu_6Sn_5 and Cu_3Sn.

Structure	A^U	A_{comp}	A_{shear}	A_1	A_2	A_3
η′-Cu_6Sn_5	0.0848	0.0066	0.0071	0.9210	0.9545	1.0455
Cu_3Sn	0.0838	0.0022	0.0079	1.0847	1.1164	1.0574

To reveal the elastic anisotropy more concretely, the directional dependences of *E*, *B*, and *G* were obtained, and the results are exhibited as three-dimensional (3D) surfaces in Cartesian coordinates. Furthermore, the deviation between the 3D surfaces and the sphere shape denotes the degree of anisotropy. The 3D surfaces of *E* can be obtained by Equation (17) [43] as follows:

$$1/E(\mathbf{n}) = S_{11}n_1^4 + S_{22}n_2^4 + S_{33}n_3^4 + (S_{44}+2S_{23})n_2^2n_3^2 + (S_{55}+2S_{31})n_3^2n_1^2 + (S_{66}+2S_{12})n_1^2n_2^2 + 2n_2n_3[(S_{14}+S_{56})n_1^2 + S_{24}n_2^2 + S_{34}n_3^2] + 2n_3n_1[S_{15}n_1^2 + (S_{25}+S_{46})n_2^2 + S_{35}n_3^2] + 2n_1n_2[S_{16}n_1^2 + S_{26}n_2^2 + (S_{36}+S_{45})n_3^2] \quad (17)$$

where n_1, n_2, and n_3 denote the directional cosines of loading-direction **n** with three principal directions. For the two IMCs, the 3D surfaces and their cross-sections of E are illustrated in Figures 2 and 3, respectively. In this study, anisotropy ratio E_{max}/E_{min} was employed to quantify the amount of anisotropy; the larger the anisotropy ratio, the higher the anisotropy [44]. For η′-Cu_6Sn_5, E_{max} = 124.6 GPa, E_{min} = 89.5 GPa, and the anisotropy ratio was 1.39. The directions of E_{max} and E_{min} were (1, 0, −0.76) and (1, 0, 0.42), respectively. The anisotropic ratios, maximum and minimum values of E is listed Table 6 for η′-Cu_6Sn_5 and Cu_3Sn. Obviously, E anisotropy in the xz plane was the highest for η′-Cu_6Sn_5. For Cu_3Sn, the results showed that the 3D plot of E was non-spherical (see Figure 2b); moreover, E_{max} and E_{min} were 153.9 GPa and 116.0 GPa, respectively. The anisotropy ratio was 1.33, and the directions of E_{max} and E_{min} were (1, 0.84, 0) and (0, 0, 1), respectively. It is noted that E anisotropy of the yz and xz planes was similar for Cu_3Sn. Overall, the anisotropy ratio of η′-Cu_6Sn_5 was higher, which showed that E anisotropy of η′-Cu_6Sn_5 was higher. This conclusion is also supported by the A^U values shown in Table 5. Furthermore, the 3D surfaces of G could be obtained by the following formula [43]:

$$\begin{aligned}1/G(\mathbf{n},\mathbf{m}) = {} & 4[2S_{12} - (S_{11}+S_{22}-S_{66})]n_1m_1n_2m_2 + 4[2S_{23} - (S_{22}+S_{33}-S_{44})]n_2m_2n_3m_3 \\ & + 4[2S_{31} - (S_{33}+S_{11}-S_{55})]n_3m_3n_1m_1 + 4(n_1m_2+n_2m_1)[(S_{16}-S_{36})n_1m_1 + (S_{26}-S_{36})n_2m_2] \\ & + 4(n_2m_3+n_3m_2)[(S_{24}-S_{14})n_2m_2 + (S_{34}-S_{14})n_3m_3] \\ & + 4(n_3m_1+n_1m_3)[(S_{35}-S_{25})n_3m_3 + (S_{15}-S_{25})n_1m_1] \\ & + S_{44}(n_2m_3-n_3m_2)^2 + S_{55}(n_3m_1-n_1m_3)^2 + S_{66}(n_1m_2-n_2m_1)^2 \\ & + 2S_{45}(n_2m_3+n_3m_2)(n_3m_1+n_1m_3) \\ & + 2S_{56}(n_3m_1+n_1m_3)(n_1m_2+n_2m_1) + 2S_{64}(n_1m_2+n_2m_1)(n_2m_3+n_3m_2)\end{aligned} \quad (18)$$

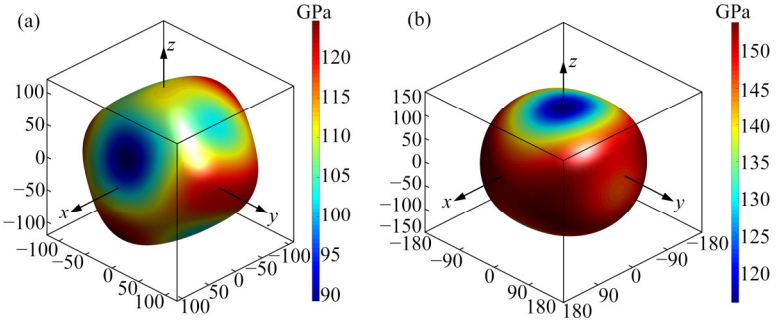

Figure 2. The 3D directional dependence of E for (**a**) η′-Cu_6Sn_5, (**b**) Cu_3Sn.

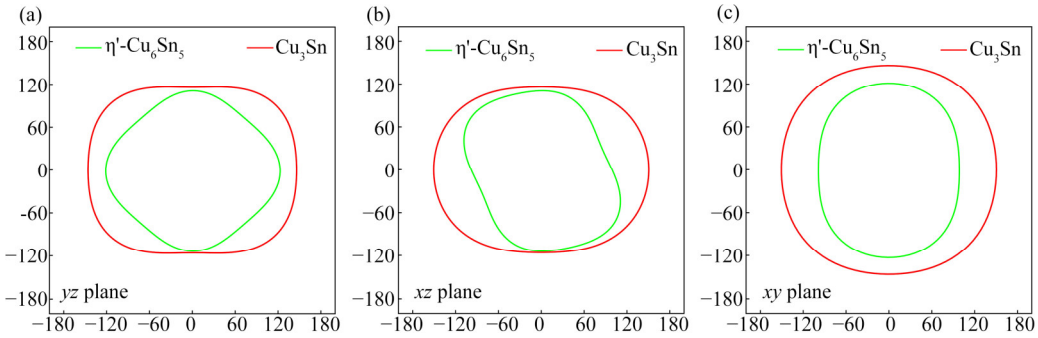

Figure 3. Cross-sections of E in the yz, xz, and xy planes for η′-Cu_6Sn_5 and Cu_3Sn: (**a**) the yz plane; (**b**) the xz plane; (**c**) the xy plane. The green and red lines denote the cross-sections for η′-Cu_6Sn_5 and Cu_3Sn, respectively.

Table 6. The anisotropic ratios, maximum and minimum values of *E* for η′-Cu_6Sn_5 and Cu_3Sn.

	η′-Cu_6Sn_5				Cu_3Sn			
	Whole	***yz***	***xz***	***xy***	**Whole**	***yz***	***xz***	***xy***
E_{max} (GPa)	124.6	122.1	124.6	122.1	153.9	149.7	150.6	177.8
E_{min} (GPa)	89.5	103.2	89.5	98.7	116.0	116.0	116.0	125.1
Anisotropic ratios	1.39	1.18	1.39	1.24	1.33	1.29	1.30	1.42

where m_1, m_2, and m_3 are the directional cosines of measurement direction **m**, and **m** is perpendicular to **n**. In a particular direction **n**, *G* will be changed with a change in **m**. For the two IMCs, the directional dependences of maximum and minimum *G* are plotted in Figure 4. In addition, the cross-sections of maximum and minimum *G* in the *yz*, *xz*, and *xy* planes are shown in Figure 5. In this study, anisotropy ratio G_{max}/G_{min} was employed to describe the anisotropic degree of *G*. For η′-Cu_6Sn_5, the directions of G_{max} = 48.3 GPa and G_{min} = 36.6 GPa were (0.71, 1, −0.71) and (−0.67, 0.60, −1), respectively; hence, the anisotropy ratio was 1.32. The anisotropic ratios, maximum and minimum values of *G* is listed Table 7 for η′-Cu_6Sn_5 and Cu_3Sn. The anisotropic degree of η′-Cu_6Sn_5 was similar in the *yz*, *xz*, and *xy* planes. For Cu_3Sn, G_{max} = 63.1 GPa, G_{min} = 46.1 GPa, and the G_{max}/G_{min} was 1.37 for Cu_3Sn. The directions of G_{max} and G_{min} were (0, 1, 0) and (0, 1, 1), respectively. Obviously, *G* anisotropy of the *yz*, *xz*, and *xy* planes was similar for Cu_3Sn.

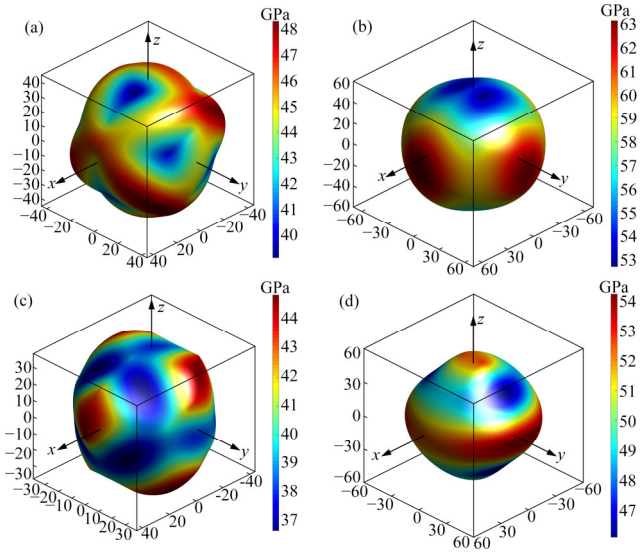

Figure 4. The 3D directional dependence of *G*: (**a**) the maximum *G* of η′-Cu_6Sn_5; (**b**) the maximum *G* of Cu_3Sn; (**c**) the minimum *G* of η′-Cu_6Sn_5; (**d**) the minimum *G* of Cu_3Sn.

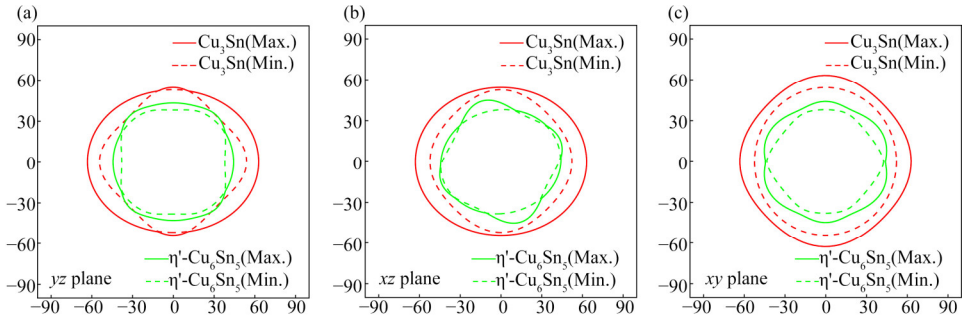

Figure 5. Cross-sections of *G* in the *yz*, *xz*, and *xy* planes for η′-Cu_6Sn_5 and Cu_3Sn: (**a**) the *yz* plane; (**b**) the *xz* plane; (**c**) the *xy* plane. The solid and dotted lines denote the maximum and minimum values, respectively. The green and red lines denote the cross-sections for η′-Cu_6Sn_5 and Cu_3Sn, respectively.

Table 7. The anisotropic ratios, maximum and minimum values of *G* for η′-Cu_6Sn_5 and Cu_3Sn.

	η′-Cu_6Sn_5				Cu_3Sn			
	Whole	***yz***	***xz***	***xy***	**Whole**	***yz***	***xz***	***xy***
G_{max} (GPa)	48.3	46.6	46.6	47.0	63.1	63.1	63.1	63.1
G_{min} (GPa)	36.6	38.0	38.0	37.2	46.1	48.9	48.9	52.3
Anisotropic ratios	1.32	1.23	1.23	1.26	1.37	1.29	1.29	1.21

In summary, for the two IMCs, *G* anisotropy of Cu_3Sn was higher. This conclusion is also supported by the A_{shear} values shown in Table 5. Finally, the directional dependences of *B* are described by formula (19) [45].

$$\begin{aligned} 1/B(\mathbf{n}) = {} & (S_{11}+S_{12}+S_{13})n_1^2 + (S_{16}+S_{26}+S_{36})n_1n_2 + (S_{15}+S_{25}+S_{35})n_3n_1 \\ & + (S_{12}+S_{22}+S_{23})n_2^2 + (S_{14}+S_{24}+S_{34})n_2n_3 \\ & + (S_{13}+S_{23}+S_{33})n_3^2 \end{aligned} \quad (19)$$

The directional dependence of *B* is shown in Figure 6. The cross-sections of *B* in the *yz*, *xz*, and *xy* planes are shown in Figure 7. Anisotropy ratio B_{max}/B_{min} was performed to describe the anisotropic degree of *B*. For η′-Cu_6Sn_5, B_{max} = 354.2 GPa was located on the *yz* and *xy* planes, and the B_{min} = 206.1 GPa was located on the *xz* planes. The anisotropy ratio was 1.72, and the directions of B_{max} and B_{min} were (0, 1, 0) and (1, 0, 0.67), respectively. The anisotropic ratios, maximum and minimum values of *B* is listed Table 8 for η′-Cu_6Sn_5 and Cu_3Sn. The *B* anisotropy of η′-Cu_6Sn_5 was found to be the highest in the *xy* plane. For Cu_3Sn, B_{max} = 480.7 GPa, B_{min} = 343.9 GPa, and the anisotropy ratio was 1.40. The directions of B_{max} and B_{min} were (0, 1, 0) and (0, 0, 1), respectively. The anisotropic degree of *B* was highest in the *yz* plane of Cu_3Sn. It is noted that *B* anisotropy of η′-Cu_6Sn_5 was higher than Cu_3Sn, which can be confirmed by A_{comp} (see Table 5).

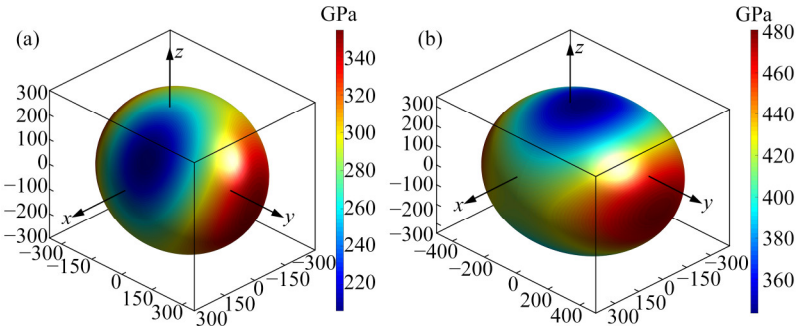

Figure 6. The 3D directional dependence of *B*: (**a**) η′-Cu_6Sn_5; (**b**) Cu_3Sn.

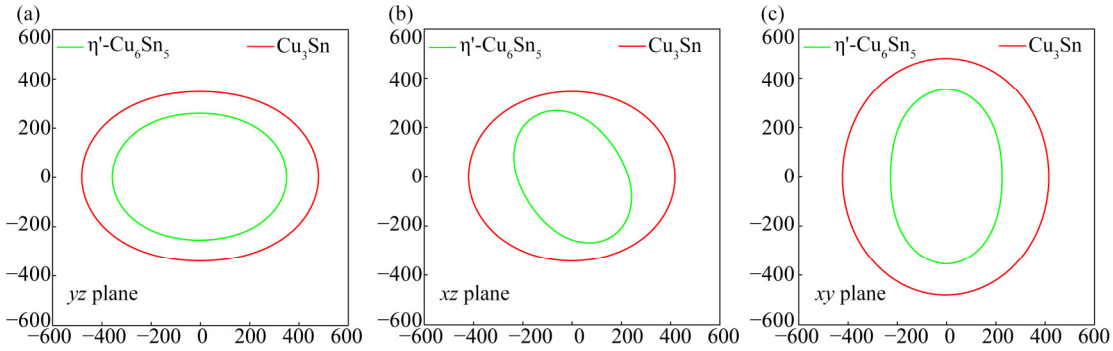

Figure 7. Cross-sections of *B* in the *yz*, *xz*, and *xy* planes for η′-Cu_6Sn_5 and Cu_3Sn: (**a**) the *yz* plane; (**b**) the *xz* plane; (**c**) the *xy* plane. The green and red lines denote the cross-sections of η′-Cu_6Sn_5 and Cu_3Sn, respectively.

Table 8. The anisotropic ratios, maximum and minimum values of *B* for η′-Cu_6Sn_5 and Cu_3Sn.

	η′-Cu_6Sn_5				**Cu_3Sn**			
	Whole	***yz***	***xz***	***xy***	**Whole**	***yz***	***xz***	***xy***
B_{max} (GPa)	354.2	354.2	289.9	354.2	480.7	480.7	419.0	480.7
B_{min} (GPa)	206.1	257.3	206.1	226.4	343.9	343.9	343.9	418.9
Anisotropic ratios	1.72	1.38	1.41	1.56	1.40	1.40	1.22	1.15

4. Conclusions

Clarifying the mechanical properties of IMCs is helpful to provide basic material properties for finite element analysis and improve the reliability of microscale solder joints. In this work, the mechanical properties and elastic anisotropies of η′-Cu_6Sn_5 and Cu_3Sn were investigated using the first-principles calculations method. The conclusions of the present work are as follows.

1. For η′-Cu_6Sn_5 and Cu_3Sn, the elastic constants of single crystals and polycrystalline aggregates were obtained using first-principles calculations. Accordingly, *E*, *G*, *B*, and *ν* of the two IMCs all exhibited the following relationship: Cu_3Sn > η′-Cu_6Sn_5. Moreover, the values of *G*/*B* and *ν* showed that the two IMCs were ductile materials.
2. The directional dependence analysis of *E* had anisotropy ratios of 1.39 and 1.33 for monocrystalline η′-Cu_6Sn_5 and Cu_3Sn, respectively. The *E* anisotropy reflected the following relationship: η′-Cu_6Sn_5 > Cu_3Sn.
3. The two monocrystalline IMCs exhibited evident anisotropy of *G*; the anisotropy ratios were 1.32 and 1.37 for η′-Cu_6Sn_5, and Cu_3Sn, respectively. Accordingly, *G* anisotropy abided by the following relationship: Cu_3Sn > η′-Cu_6Sn_5. In addition, the anisotropic degree of *E* and *G* was similar for η′-Cu_6Sn_5 and Cu_3Sn.
4. For *B* of the two monocrystalline IMCs, the anisotropy ratio of η′-Cu_6Sn_5 was higher, reaching 1.72. For Cu_3Sn, the anisotropy ratios were 1.40. The relationship for *B* anisotropy was η′-Cu_6Sn_5 > Cu_3Sn. Furthermore, the anisotropy of *B* was higher compared with *G* and *E* for η′-Cu_6Sn_5; however, in the case of Cu_3Sn, the anisotropic degree of *B*, *G*, and *E* was similar.

Author Contributions: Conceptualization, H.Q. and C.D.; methodology, C.D., J.W. and T.L.; software, C.D., J.W. and T.L.; validation, H.Q.; formal analysis, C.D. and J.W.; data curation, H.Q. and C.D.; writing—original draft preparation, H.Q. and C.D.; writing—review and editing, D.Y. and G.Z.; supervision, H.Q., D.Y. and G.Z.; project administration, H.Q.; funding acquisition, H.Q. All authors have read and agreed to the published version of the manuscript.

Funding: This study was sponsored by the National Natural Science Foundation of China (NSFC) under grant. Nos. 51505095, 51805103 and No. 52065015; Guangxi Natural Science Foundation under grant. Nos. 2018GXNSFAA281222 and 2021 GXNSFAA075010; Science and Technology Planning Project of Guangxi Province under Grant Nos. GuiKeAD AD18281022 and 18281021, Director Fund Project of Guangxi Key Laboratory of Manufacturing System and Advanced Manufacturing Technology Nos. 19-050-44-003Z and 20-065-40-002Z, Self-Topic Fund of Engineering Research Center of Electronic Information Materials and Devices Nos. EIMD-AB202005 and EIMD-AB202001. Innovation Project of GUET Graduate Education under grant No. 2020YCXS001 and 2021YCXS006.

Institutional Review Board Statement: Not applicable.

Informed Consent Statement: Not applicable.

Data Availability Statement: Data are available from the corresponding author on request.

Acknowledgments: The author thanks the Engineering Research Center of Electronic Information Materials and Devices and Guangxi Key Laboratory of Manufacturing System and Advanced Manufacturing Technology for their support in the research.

Conflicts of Interest: The authors declare no conflict of interest.

References

1. Liu, X.; He, S.; Nishikawa, H. Thermally stable Cu 3 Sn/Cu composite joint for high-temperature power device. *Scr. Mater.* **2016**, *110*, 101–104, doi:10.1016/j.scriptamat.2015.08.011.
2. Sun, F.; Pan, Z.; Liu, Y. The fracture mechanism of Cu3Sn-microporous copper composite joint by thermal compression bonding process. *Mater. Lett.* **2021**, *291*, 129536, doi:10.1016/j.matlet.2021.129536.
3. Yao, P.; Li, X.; Han, X.; Xu, L. Shear strength and fracture mechanism for full Cu-Sn IMCs solder joints with different Cu3Sn proportion and joints with conventional interfacial structure in electronic packaging. *Solder. Surf. Mt. Technol.* **2019**, *31*, 6–19, doi:10.1108/ssmt-06-2018-0018.
4. Ghosh, G.; Asta, M. Phase Stability, Phase Transformations, and Elastic Properties of Cu6Sn5: Ab initio Calculations and Experimental Results. *J. Mater. Res.* **2005**, *20*, 3102–3117, doi:10.1557/jmr.2005.0371.
5. Gao, F.; Qu, J.; Takemoto, T. Additive Occupancy in the Cu6Sn5-Based Intermetallic Compound Between Sn-3.5Ag Solder and Cu Studied Using a First-Principles Approach. *J. Electron. Mater.* **2010**, *39*, 426–432, doi:10.1007/s11664-010-1093-8.
6. Hu, X.; Xu, T.; Keer, L.M.; Li, Y.; Jiang, X. Shear strength and fracture behavior of reflowed Sn3.0Ag0.5Cu/Cu solder joints under various strain rates. *J. Alloy. Compd.* **2017**, *690*, 720–729, doi:10.1016/j.jallcom.2016.08.168.
7. Wan, Y.; Li, S.; Hu, X.; Qiu, Y.; Xu, T.; Li, Y.; Jiang, X. Shear strength and fracture surface analysis of Sn58Bi/Cu solder joints under a wide range of strain rates. *Microelectron. Reliab.* **2018**, *86*, 27–37, doi:10.1016/j.microrel.2018.05.007.
8. Zhu, W.; Shi, L.; Jiang, L.; He, H. Effect of intermetallic compound thickness on mechanical fatigue properties of copper pillar micro-bumps. *Microelectron. Reliab.* **2020**, *111*, 113723, doi:10.1016/j.microrel.2020.113723.
9. Tian, Y.; Han, J.; Ma, L.; Guo, F. The dominant effect of c-axis orientation in tin on the electromigration behaviors in tricrystal Sn-3.0Ag-0.5Cu solder joints. *Microelectron. Reliab.* **2018**, *80*, 7–13, doi:10.1016/j.microrel.2017.11.005.
10. Qiu, H.; Hu, X.; Li, S.; Wan, Y.; Li, Q. Shear strength and fracture surface analysis of lead-free solder joints with high fraction of IMCs. *Vacuum.* **2020**, *180*, 109611, doi:10.1016/j.vacuum.2020.109611.
11. Yin, Z.; Sun, F.; Guo, M. Investigation of Elevated Temperature Mechanical Properties of Intermetallic Compounds in the Cu–Sn System Using Nanoindentation. *J. Electron. Packag.* **2020**, *142*, 021004, doi:10.1115/1.4045980.
12. Song, J.-M.; Huang, B.-C.; Tarng, D.; Hung, C.-P.; Yasuda, K. Relationship between Nanomechanical Responses of Interfacial Intermetallic Compound Layers and Impact Reliability of Solder Joints. *Nanomaterials* **2020**, *10*, 1456, doi:10.3390/nano10081456.
13. Zhang, A.; Peng, P.; Zheng, W.; Yang, J.; Zhang, X.; Xu, Y. Phase selection and nano-mechanical properties of intermetallic compounds in directionally solidified Cu-68at.%Sn peritectic alloy. *J. Alloys Compd.* **2021**, *859*, 157866, doi:10.1016/j.jallcom.2020.157866.
14. Ghosh, G. Elastic properties, hardness, and indentation fracture toughness of intermetallics relevant to electronic packaging. *J. Mater. Res.* **2004**, *19*, 1439–1454, doi:10.1557/jmr.2004.0193.
15. An, R.; Wang, C.; Tian, Y.; Wu, H. Determination of the Elastic Properties of Cu3Sn Through First-Principles Calculations. *J. Electron. Mater.* **2008**, *37*, 477–482, doi:10.1007/s11664-007-0358-3.
16. Mu, D.; Huang, H.; Nogita, K. Anisotropic mechanical properties of Cu6Sn5 and (Cu,Ni)6Sn5. *Mater. Lett.* **2012**, *86*, 46–49, doi:10.1016/j.matlet.2012.07.018.
17. Choudhury, S.F.; Ladani, L. Grain Growth Orientation and Anisotropy in Cu6Sn5 Intermetallic: Nanoindentation and Electron Backscatter Diffraction Analysis. *J. Electron. Mater.* **2014**, *43*, 996–1004, doi:10.1007/s11664-014-2977-9.
18. Ortiz, A.U.; Boutin, A.; Fuchs, A.; Coudert, F.X. Anisotropic Elastic Properties of Flexible Metal-Organic Frameworks: How Soft are Soft Porous Crystals? *Phys. Rev. Lett.* **2012**, *109*, 195502, doi:10.1103/physrevlett.109.195502.
19. Wen, Y.; Zeng, X.; Hu, Z.; Peng, R.; Sun, J.; Song, L. A comparative first-principles study of tetragonal TiAl and Ti4Nb3Al9 intermetallic compounds. *Intermetallics* **2018**, *101*, 72–80, doi:10.1016/j.intermet.2018.07.012.
20. Zhang, X.; Zhao, X.; Zheng, B.; Liu, Y.; Cheng, J.; Li, H. First-Principles Study of Thermodynamical and Elastic Properties of η′-(Cu,Co)6Sn5 Ternary Alloys. *J. Electron. Mater.* **2016**, *45*, 4919–4927, doi:10.1007/s11664-016-4654-7.
21. Zhang, W.W.; Lin, X.; Mao, Z.; Wu, P. The structural, elastic, thermodynamic, and electronic properties of (Cu6-xAux)Sn5 (x = 0, 0.5, 1, 1.5, 2) intermetallic compounds. *Indian J. Phys.* **2020**, *95*, 1–7, doi:10.1007/s12648-020-01918-w.
22. Huang, W.; Pan, K.; Zhang, J.; Gong, Y. Effect of In-Doping on Mechanical Properties of Cu6Sn5-Based Intermetallic Compounds: A First-Principles Study. *J. Electron. Mater.* **2021**, *50*, 4165–4171, doi:10.1007/s11664-021-08929-1.
23. Leineweber, A.; Löffler, M.; Martin, S. Stable and Metastable Phase Equilibria Involving the Cu6Sn5 Intermetallic. *J. Electron. Mater.* **2021**, *50*, 5898–5914, doi:10.1007/s11664-021-09067-4.
24. Nogita, K.; Gourlay, C.M.; McDonald, S.D.; Wu, Y.Q.; Read, J.; Gu, Q.F. Kinetics of the η–η′ transformation in Cu6Sn5. *Scr. Mater.* **2011**, *65*, 922–925.
25. Segall, M.D.; Lindan, P.J.D.; Probert, M.; Pickard, C.J.; Hasnip, P.; Clark, S.; Payne, M.C. First-principles simulation: ideas, illustrations and the CASTEP code. *J. Physics: Condens. Matter* **2002**, *14*, 2717–2744, doi:10.1088/0953-8984/14/11/301.
26. Segall, M.D.; Probert, M.J.; Pickard, C.J.; Hasnip, P.J.; Clark, S.J.; Refson, K.; Yates, J.R.; Payne, M.C. *Materials Studio CASTEP Version 8.0*; Cambridge University and Accelrys Inc: Cambridge, UK, 2000.
27. Burkhardt, W.; Schubert, K. Über messingartige Phasen mit A3-verwandter Struktur. *Int. J. Mater. Res.* **1959**, *50*, 442–452, doi:10.1515/ijmr-1959-500802.
28. Larsson, A.; Stenberg, L.; Lidin, S. The superstructure of domain-twinned η′-Cu6Sn5. *Acta Crystallogr. Sect. B Struct. Sci.* **1994**, *50*, 636–643, doi:10.1107/s0108768194004052.
29. Perdew, J.P.; Burke, K.; Ernzerhof, M. Generalized gradient approximation made simple. *Phys. Rev. Lett.* **1996**, *77*, 3865–3868.

30. Vanderbilt, D. Soft self-consistent pseudopotentials in a generalized eigenvalue formalism. *Phys. Rev. B* **1990**, *41*, 7892–7895, doi:10.1103/physrevb.41.7892.
31. Wang, Y.; Dong, Y.; Zhao, X.; Huo, Y.; Liu, Y. A first-principles computation-driven mechanism study on the solders dilute doping effects to η′-Cu6Sn5 growth kinetics. *J. Mater. Sci.* **2021**, *56*, 9741–9753, doi:10.1007/s10853-020-05702-3.
32. Jiang, L.; Muthegowda, N.; Bhatia, M.; Migliori, A.; Solanki, K.; Chawla, N. Full elastic constants of Cu 6 Sn 5 intermetallic by Resonant Ultrasound Spectroscopy (RUS) and ab initio calculations. *Scr. Mater.* **2015**, *107*, 26–29, doi:10.1016/j.scriptamat.2015.05.012.
33. Qu, D.; Li, C.; Bao, L.; Kong, Z.; Duan, Y. Structural, electronic, and elastic properties of orthorhombic, hexagonal, and cubic Cu3Sn intermetallic compounds in Sn–Cu lead-free solder. *J. Phys. Chem. Solids* **2020**, *138*, 109253, doi:10.1016/j.jpcs.2019.109253.
34. Singh, S.; Lang, L.; Dovale-Farelo, V.; Herath, U.; Tavazohi, P.; Coudert, F.-X.; Romero, A.H. MechElastic: A Python Library for Analysis of Mechanical and Elastic Properties of Bulk and 2D Materials. *Comput. Phys. Commun.* **2021**, *267*, 108068, doi:10.1016/j.cpc.2021.108068.
35. Pang, X.; Wang, S.; Zhang, L.; Liu, Z.; Shang, J. First principles calculation of elastic and lattice constants of orthorhombic Cu3Sn crystal. *J. Alloys Compd.* **2008**, *466*, 517–520, doi:10.1016/j.jallcom.2007.11.095.
36. Guechi, N.; Bouhemadou, A.; Khenata, R.; Bin-Omran, S.; Chegaar, M.; Al-Douri, Y.; Bourzami, A. Structural, elastic, electronic and optical properties of the newly synthesized monoclinic Zintl phase BaIn2P2. *Solid State Sci.* **2014**, *29*, 12–23, doi:10.1016/j.solidstatesciences.2014.01.001.
37. Zhang, P.; Ma, Z.; Wang, Y.; Zou, Y.; Lei, W.; Pan, Y.; Lu, C. A first principles study of the mechanical properties of Li–Sn alloys. *RSC Adv.* **2015**, *5*, 36022–36029, doi:10.1039/c5ra04685h.
38. Qin, H.; Luan, X.; Feng, C.; Yang, D.; Zhang, G. Mechanical, Thermodynamic and Electronic Properties of Wurtzite and Zinc-Blende GaN Crystals. *Materials* **2017**, *10*, 1419, doi:10.3390/ma10121419.
39. Hill, R. The Elastic Behaviour of a Crystalline Aggregate. *Proc. Phys. Soc. Sect. A* **1952**, *65*, 349–354, doi:10.1088/0370-1298/65/5/307.
40. Chromik, R.; Vinci, R.; Allen, S.L.; Notis, M.R. Nanoindentation measurements on Cu–Sn and Ag–Sn intermetallics formed in Pb-free solder joints. *J. Mater. Res.* **2003**, *18*, 2251–2261, doi:10.1557/jmr.2003.0314.
41. Chen, J.; Lai, Y.S.; Yang, P.F. First-Principles Calculations of Elastic Properties of Cu3Sn and Cu6Sn5 intermetallics. *IEEE Trans. Adv. Packag.* **2009**, *32*, 754–757, doi:10.1109/tadvp.2009.2012726.
42. Bai, C.G.; Chai, C.C.; Fan, Q.Y.; Liu, Y.Q.; Yang, Y.T. A novel silicon allotrope in the monoclinic phase. *Materials* **2017**, *10*, 441.
43. Ting, T.C.T. On anisotropic elastic materials for which Young's Modulus E(n) is independent of n or the Shear Modulus G(n,m) is independent of n and m. *J. Elast.* **2006**, *81*, 271–292.
44. Gomis, O.; Manjón, F.; Rodríguez-Hernández, P.; Muñoz, A. Elastic and thermodynamic properties of α-Bi2O3 at high pressures: Study of mechanical and dynamical stability. *J. Phys. Chem. Solids* **2019**, *124*, 111–120, doi:10.1016/j.jpcs.2018.09.002.
45. Nye, J.F. *Physical Properties of Crystals*; Oxford University Press: New York, NY, USA, 1985; p. 146.